

Shahid Chamran
University of Ahvaz

Journal of Applied and Computational Mechanics



Research Paper

Thermal Behavior of Monocrystalline Silicon Solar Cells: A Numerical and Experimental Investigation on the Module Encapsulation Materials

Ana Pavlovic¹, Cristiano Fragassa¹, Marco Bertoldi², Vladyslav Mikhnych³¹ University of Bologna (UNIBO), Department of Industrial Engineering, Via Fontanelle 40, Forlì, Italy, Emails: ana.pavlovic@unibo.it; cristiano.fragassa@unibo.it² University of Bologna (UNIBO), Department of Electrical, Energy and Information Engineering "Guglielmo Marconi", Viale del Risorgimento 2, Bologna, Italy, Email: m.bertoldi@unibo.it³ Karlsruhe Institute of Technology (KIT), Karlsruhe School of Optics & Photonics, Schloßpl. 19, 76131 Karlsruhe, Germany, Email: vladyslav.mikhnych@studio.unibo.it

Received June 29, 2021; Revised July 10 2021; Accepted for publication July 11 2021.

Corresponding author: C. Fragassa (cristiano.fragassa@unibo.it)

© 2021 Published by Shahid Chamran University of Ahvaz

Abstract. This research outlines the numerical predictions of the heat distribution in solar cells, accompanied by their empirical validation. Finite element thermal models of five laminated silicon solar photovoltaic cells were firstly established using a simulation software (ANSYS®). The flexible laminated solar cells under study are made of a highly transparent frontsheet, a silicon cell between two encapsulants, and a backsheet. Different combinations of layers (i.e., materials and thicknesses) were taken into account in order to analyze their effect on thermal behavior. Thermal properties of materials were derived in accordance with the literature. Similarly, boundary conditions, loads, and heat losses by reflection and convection were also specified. The solar cells were tested using solar lamps under standard conditions (irradiance: 1000W/m²; room-temperature: 25°C) with real-time temperatures measured by a thermal imager. This analysis offers an interpretation of how temperature evolves through the solar cell and, consequently, how the design choice can influence the cells' efficiency.

Keywords: Photovoltaics, Solar Mobility, Solar Cell Efficiency, Transient Thermal Analysis, Finite Elements.

1. Introduction

In order to reduce urban pollution and global warming, electric vehicles can represent an effective and powerful option [1], especially when their energy derives from alternative and sustainable sources [2]. An intriguing option is represented by the emerging solar vehicles [3]: electrical vehicles powered by solar energy provided by the photovoltaic (PV) panels, typically located on the roof [4]. Solar cars circulating on the roads can still be counted on the fingers of the hands nowadays, but there are many sophisticated prototypes in the numerous competitions for solar vehicles worldwide [5]. Their race performance highly depends on the efficiency of the PV panels in converting sunlight into electricity thanks to light-absorbing materials (i.e., monocrystalline, polycrystalline or amorphous silicon, gallium arsenide, organic compounds, etc.) [6, 7]. Several factors affect the PV conversion efficiency as reflectance, thermodynamic efficiency, charge carrier separation efficiency, charge carrier collection efficiency and conduction efficiency. The world record for solar cell efficiency at 47.1% was achieved in 2019 by using multi-junction concentrator solar cells [8], but, typically, values are much lower.

Many solar cars use monocrystalline silicon, with cells entirely based around the concept of a *p-n junction*. Monocrystalline silicon (c-Si) technology introduces a single-crystal structure that enables electrons to move easier than in a multi-crystal configuration. These cells are made from wafers between 160 and 240 micrometers thick, then protected by laminating them between with a highly transparent frontsheet, two encapsulants, and a backsheet in a process called 'encapsulation'. Everything is made for improving the overall efficiency [9].

Theoretically, the thermodynamic efficiency limit, equal to the absolute maximum possible conversion efficiency of sunlight to electricity, is about 86%. This value represents an approximation (i.e., Chambadal-Novikov efficiency) related to the Carnot limit and is based on the temperature of the photons emitted by the Sun's surface. On the contrary, the real thermodynamic efficiency limit is much lower at around 33% in the case of a single junction technology. This means that the conversion efficiency does not exceed 12-21% in the case of commercial PV panels or up to 24.5% for high-performance single junction cells, frequently preferred for solar race vehicles [10].

Moreover, it is largely known that the PV conversion efficiency is strictly related to the cells operating temperature [11]. For instance, in [12] it was found that the efficiency decreases by 0.38-0.42% (i.e., relative percentage) and in [13] that the electrical



power falls by 0.4-0.5% every 1 degree of temperature growth in the silicon cells. A conventional simplification is to consider a linear drop in panel efficiency of 1% (i.e., absolute percentage) every 10 degrees [14]. Therefore, even marginal changes (<4-5 °C) in terms of temperatures can clearly affect the overall performance ($\approx 0.3-0.4\%$) and benefits can be achieved acting on the encapsulation in terms of materials and processes. This was the technical argument that prompted the implementation of the present investigation.

For this reason, it was necessary to investigate the thermal behavior of laminates which can be known by transient thermal simulations and proper numerical models, better when validated by experiments. Then, from the cell temperature, the efficiency of the solar panel can be obtained thanks to empirical relationships characteristic of each type of solar cell and known with high accuracy ($\pm 0.25\%$).

The state of the art also suggests recent efforts in thermal modeling of solar cells ([15]), each one characterized by its own features, even including experiments [16] or solar cars [17]. In [18], e.g., a swarm optimization algorithm is proposed for calculating the temperature inside the PV module merging thermal and electrical properties. Besides, the closest investigation in terms of objectives and methods with respect to the present one is maybe [19] where the cell temperature distribution in the PV module was estimated by applying computational fluid dynamics (CFD) and finite element method (FEM). A three-dimensional thermal model was implemented, and the temperature distribution of the cell layer and module's thickness direction were simulated. Among other useful information, the temperature distribution curves showed that the silicon layer possessed the highest temperature, and that this temperature is located near the solar cell center.

Similar approaches for investigating the thermal performance of solar cells were also proposed in [20] and [21]. Where they differ is that the first research was focused on the high-concentration PV solar package while the second one was based on electronic packages.

However, none of the mentioned works directly combines all specific aspects characterizing the present paper regarding the panel (i.e., monocrystalline silicon, advanced materials for encapsulation, additional layers for structural purposes, material alternatives) and methods (i.e., thermal transient analysis, absence of CFD dissipative effects, experimental validation). In the current research, in fact, we first built a detailed 3D finite-element model of the monocrystalline silicon solar cells using ANSYS software and performed the numerical analysis, then we performed experiments by infrared (IR) thermography in order to validate the FEM model. In this process, several alternative layouts of solar panels were considered with the scope to investigate the effect of design changes (i.e., the stacking sequences) in terms of thermal behavior and efficiency, before incorporating them on a solar vehicle [22-24].

2. Materials

2.1. Solar cells

Monocrystalline solar cells (125X125mm, diameter 150mm, pseudo-square with rounded corners) manufactured by KPE were considered. As technical dimensions they present wafer edge length of $125 \pm 0.5\text{mm}$, wafer thickness of $200-220 \pm 30\mu\text{m}$, minimum and maximum lengths (corner to corner) of 149 and 151mm, flake type chips width and depth of 1.5 and 0.5mm, number of flake type chips allowed ≤ 2 per Solar Cell. As electrical parameters, the selected grade (i.e., PS1) offers a conversion efficiency of $17.25\% \pm 0.25\%$ and a maximum peak power of $2.56 \pm 0.05 \text{ Wp}$ measured with respect to standard conditions ($1,000 \text{ W/m}^2$, AM 1.5G, 25°C). Finally, the corners of the cells look clipped, like an octagon, because the monocrystal silicon is cut from cylindrical ingots that are typically grown by the Czochralski process.

2.2. Laminate layering

A solar panel using silicon cells is commonly made laminating:

- ✓ Glass (or ETFE)
- ✓ EVA
- ✓ Mono (or polycrystalline) silicon cells
- ✓ EVA
- ✓ PET (or Glass)

The glass is used as a protecting base on which a thin ethylene-vinyl acetate (EVA) sheet is spread. This glass has a special content (i.e., low iron) to ensure the highest transparency. Then, a first EVA sheet is positioned facing with the photosensitive side down, before another EVA sheet is placed on the back of the cell and then there is a sheet of insulating plastic material as Polyethylene Terephthalate (PET) or similar. Everything is laminated in a laminator (or autoclave) where, in a vacuum environment to limit impurities and gas infiltrations, a plate placed in contact is heated up to 145°C for about ten minutes in order to sustain the polymerization of the EVA. Thanks to the vacuum, the EVA spreads homogeneously on the cells except for not-functional edges while its thickness is reduced to around $10-20 \mu\text{m}$. Then, the laminate is extracted and cells are encapsulated in the way to withstand the elements for years.

In the present case, the layout was the same except for using ethylene tetrafluoroethylene (ETFE) for frontsheet instead of glass with the scope to reduce weight, have higher transparency and make the laminated panel flexible. A sheet of ETFE is in fact equal to 2% by weight of an equivalent glass sheet. ETFE is a plastic polymer containing fluorine atoms with extraordinary properties which make it exceptionally suitable as frontsheet in solar cells: it is self-cleaning, stable, with very high resistance to corrosion, thermal excursion and atmospheric agents. Moreover, its chemical structure makes the material extremely good at allowing light radiation to pass through, almost eliminating the phenomenon of reflection. Finally, this material also offers an insulating power, useful to prevent electrical failures.

Regarding the manufacturing process, very little differences respect to the conventional procedures were introduced, simply related to the fact that a laboratory autoclave was used instead of a laminator. Some phases of the process are shown in Fig. 1.

In particular, the cell layers were positioned on a glass sheet, laid in reverse order: PET, EVA, Silicon, EVA, ETFE (Fig. 1a). This glass was introduced to provide a planar support during the autoclaving process (in a laminator this function is offered by the machine worktable) and removed at the end. A negative pressure (1 bar) was applied by means of a vacuum bag and vacuum pump with the dual purpose of structurally stabilizing the system and air extracting (Fig. 1b). The presence of air, in fact, would oppose the uniform polymerization. Then, a thermal cycle (with 120° for 90min) was applied in the autoclave permitting the EVA sheets to polymerize. Finally, after cooling (Fig. 1c) and removal from the vacuum bag, the solar panels were anchored along the edges by adhesive (i.e., double-sided tape, cod. 468MP. by 3M) to a carbon fiber composite polymer (CFRP) panel which is intended to represent the vehicle roof.



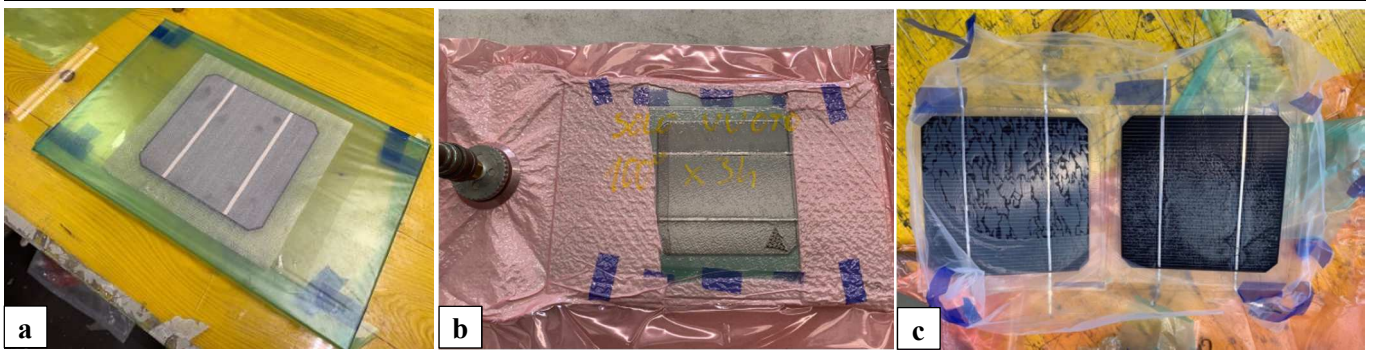


Fig. 1. Solar cell manufacturing: a) layers (ETFE, EVA, Silicon, EVA, PET) positioning on a glass sheet as support for lamination (back view); b) vacuum application (1 bar) by means of a vacuum bag and vacuum pump (back view); c) solar cells after curing in autoclave (front view).

2.3. Samples Type

The analysis involved 5 different stacking sequences (or layups), created by removing/modifying one of the expected layers (Table 1): starting from a reference layout (1st) containing all the five conventional layers (i.e., ETFE; EVA; Silicon; EVA; PET), four stratification changes were proposed removing the frontsheet (ETFE) or backsheet (PET) but also to halve the thickness of the encapsulation (EVA) or distributing it only as a frame. These stacking sequences were then anchored on a CFRP plate by a frame of double-sided tape.

2.4. Thermal properties

Following the mentioned stacking sequences, their materials' thermal properties were found (Table 2). In some cases, especially for polymers, properties from references are largely variable and, consequently, it was necessary to make a specific choice (e.g., average value) which, however, does not change the general results of the study.

3. Methods

3.1. Basics of theory

A body, as a solar panel, exposed to the sun rays, achieves a temperature higher than the environment. Its thermal equilibrium is defined by the environmental temperature (T_{env} in K), the specific heat (Q_s in W/m^2) and the body's absorption coefficient (c_a).

In our case, shown in Fig. 2, the physical system is composed by a stratification of sheets made by different materials in a way that it is not easy to identify the overall absorption coefficient.

Considerations and relationships describing the thermodynamic problem are as follows.

At first, it can be said that the system (i.e., the solar panel) is isolated from the bottom (i.e., the floor) so that the induction heat exchange towards the outside is negligible. The system is therefore closed.

As second, in thermal equilibrium, the heat transmitted from the energy source (Q_{source}) to the body is equivalent to the heat emitted by the body by its components of radiation (Q_{irr}) and convection (Q_{conv}), as formulated in eq. (1).

$$Q_{source} = Q_{conv} + Q_{irr} \tag{1}$$

Both of them are functions of the body (T_{body}) and environmental (T_{env}) temperatures.

Specifically, while convection is proportional to the differences between these temperatures in accordance with Newton's Law, expressed in eq. (2), irradiation follows a law of elevation to the fourth power in accordance with the Stefan-Boltzmann's Law, expressed in eq. (3).

$$Q_{conv} = h \cdot |T_{body} - T_{env}| \tag{2}$$

$$Q_{irr} = A_0 \cdot \sigma_0 |T_{body}^4 - T_{env}^4| \tag{3}$$

Table 1. The different layouts under investigation.

Layer	Function	Material	Thickness (mm)	Layout				
				1	2	3	4	5
1 st	FrontSheet	ETFE	0.28	⊗	⊗			⊗
2 nd	Encapsulant	EVA	0.20	⊗	⊗	⊗	∅	∅
3 rd	Solar Cell	Silicon	0.15	⊗	⊗	⊗	⊗	⊗
4 th	Encapsulant	EVA	0.20	⊗	⊗	⊗	∅	⊕
5 th	Backsheet	PET	0.20	⊗		⊗	⊗	
6 th	Adhesive	Tape	0.13	⊕	⊕	⊕	⊕	⊕
7 th	Support	CFRP	2.00	⊗	⊗	⊗	⊗	⊗

⊗ regular thickness ∅ half thickness ⊕ frame

Table 2. Physical and thermal properties of selected materials.

Materials	Density (kg/m ³)	Thermal Conductivity (W/(m·K))	Specific Heat Capacity (J/(kg·K))	References
ETFE	1730	0.24	1172	[25]
EVA	945	0.35	2090	[26-27]
Silicon	2330	148	700	[28-29]
PET	1350	0.275	1275	[30-31]
CFRP	1490	6.83	1130	[32]
Tape	1012	0.19	2000	[33]



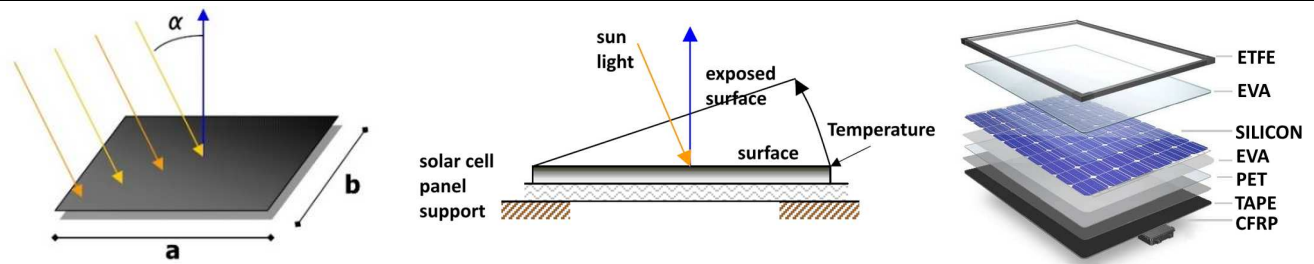


Fig. 2. Heat transfer scheme where the radiation impacts (with α angle) on a rectangular 'grey body' (with a and b dimensions) in environment, modifying its temperature. This body consists of a solar cell module, made by a stratification of different layers (ETFE, EVA, Silicon, EVA, PET), laid on a structural CFRP panel, before its positioning on supports.

The proportionality coefficients are, respectively, the heat transfer coefficient by convection (h) and the Stefan-Boltzmann constant (σ_0), equal to $5.67 \cdot 10^{-8} \text{ W/m}^2\cdot\text{k}$, multiplied by the exposed area (A_0). This area represents an orthogonal projection of the area of the irradiated body with respect to the angle of the incoming rays (α) and is related to the cosine of this angle of incidence (Lambert's cosine law). However, in the case of our experiment, $\alpha = 0$ and $\cos(\alpha) = 1$, this way the entire panel area (in m^2) can be considered. Regarding the convection coefficient (h), it is connected to several physical aspects, such as the body's geometries, the properties of the fluid (the air), including its (eventual) motion conditions. The range of values applicable to the system under testing is $h = 2.30\text{-}2.75 \text{ W/m}^2\cdot\text{k}$, definable using tables and parameters such as Nusselt and Grashof numbers, whose accurate estimate can be directly delegated to the simulation code.

Using these equations, it should be possible to identify the body temperature (T_{body}) by knowing the heat transmitted by the source (Q_{source}) and the environmental temperature (T_{env}), in our case 1000 W/m^2 and $25 \text{ }^\circ\text{C}$ respectively, when all the other (geometries, materials, etc.) factors are known. This temperature (T_{body}) can be also measured, as done in the present work for experimental validation.

Indeed, further considerations are necessary on that. Due to the fact that our panel consists of a stratification of different layers, some of them transparent, it is better to specify what the temperatures in Eq. 2 and Eq. 3 really represent.

Heat exchange is ruled by the surface temperature, while the temperature change inside the body is identified by the thermal conductivity with a thermal flux proportional to thermal gradient (Fourier's Law for heat conduction). This principle makes a redistribution of heat which also affects temperatures in ways that depend on the thermodynamic system. In the case of a homogeneous panel under sun exposure, e.g., a linear trend is obtained between a higher temperature on the exposed surface and a lower one on the hidden surface (in shadow). In the case of a solar panel, it should be also considered the fact that each layer has its own thermal conductivity, and, consequently, more complex temperature trends.

Regarding the phenomenon of diffusion, the temperature (T_{body}) in eq. (2) is represented by the temperature of the outermost layer, the one in contact with the air. This wall temperature (T_{wall}) is equivalent to the temperature of the first layer, usually represented by the frontsheet (except when the stacking sequence does not provide a frontsheet).

Regarding the phenomenon of irradiation, the temperature in eq. (3) normally refers to the same first layer. Nevertheless, the two layers above the silicon (ETFE and EVA) are almost completely transparent. Thus, T_{wall} corresponds to the temperature of the silicon this time, which also represents the temperature measured by experiments.

3.2. Numerical models

Numerical simulations were performed in Ansys Workbench® (Ver. 2020.R2) using the transient thermal analysis. This analysis was chosen, instead of steady state thermal analysis, with the scope to also investigate thermal changes over time. Moreover, CFD analysis was avoided as there are no significant fluid dynamics exchanges in the system (such as, for example, in the case of the passage of cooling air / water).

Typical thermal quantities of a transient thermal analysis are temperature distributions, heat lost or gained, thermal fluxes and so on.

Geometry models were build using the Design Modeler Module of Ansys by stacking 7 layers of $125 \times 125 \text{ mm}$, each one with proper material and thickness (Tab. 2 and 3). Specifically, five different models, one per layout, were developed. Layers were assembled considering bonded contacts which allow the complete transmission of forces and heat. The corners have been finally rounded off as in the real samples.

Discretization was implemented by SOLID186 by finite elements (FE). It is a higher-order solid element, defined by 20 nodes with 3 degrees of freedom (DoF) each (i.e., nodal translations x , y , z directions), that exhibits quadratic displacement behaviour. The system discretization was performed by (up to) 198060 nodes and 27702 elements.

Conditions and hypothesis used for the numerical thermal analysis can be summarized as follows:

- Whole radiance flux, equal to 1000 W/m^2 , impacts the panel uniformly and orthogonally.
- First layer, in ETFE reflects 7% ($= 70 \text{ W/m}^2$) and absorbs 10% ($= 100 \text{ W/m}^2$) of the transmitted irradiance.
- Remaining energy ($= 830 \text{ W/m}^2$) is applied as a constant heat flux on silicon cells (i.e., no application on EVA).
- Silicon layer reflects 3% toward ETFE ($= 25 \text{ W/m}^2$) and absorbs all the rest ($= 805 \text{ W/m}^2$).
- EVA is simplified as completely transparent matter.
- Heat is transferred between the layers by conduction.
- Heat transfer outwards occurs through ETFE and CFRP layers considering irradiation and convection phenomena.
- When ETFE is absent (3rd & 4th layouts), reflection and transmission are performed by the silicon layer.
- Emissivity, typically equal to the absorption coefficient (i.e., Kirchhoff's Law), is chosen as 0.89 for ETFE and CFRP.
- Convective heat transfer coefficient with respect to the ambient temperature is $5.67 \text{ W/m}^2\cdot\text{C}$ (eq. no wind conditions).
- Material properties are here considered independent from temperature.

3.3. Experiments

During the test, different panels were heated by appropriate equipment in controlled conditions of irradiation and environment, with temperatures measured over the entire surface. Specifically, thermal measures were done with respect to the 5 different layouts (Table 1) in 3 samples each. Tests were performed setting these 15 laminates on cardboard supports under solar lamps (fig. 3) and measuring the real-time temperatures by a thermal imager (FLIR T440®). In this way it was possible to observe not only the final equilibrium condition, but also the transition phase. The progressive increase of the panel temperature was detected over the whole surface. Standard conditions were used, with an irradiance of 1000 W/m^2 and a measured external temperature of $\approx 24.5 \text{ }^\circ\text{C}$, with changes lower than $\pm 1.5 \text{ }^\circ\text{C}$.



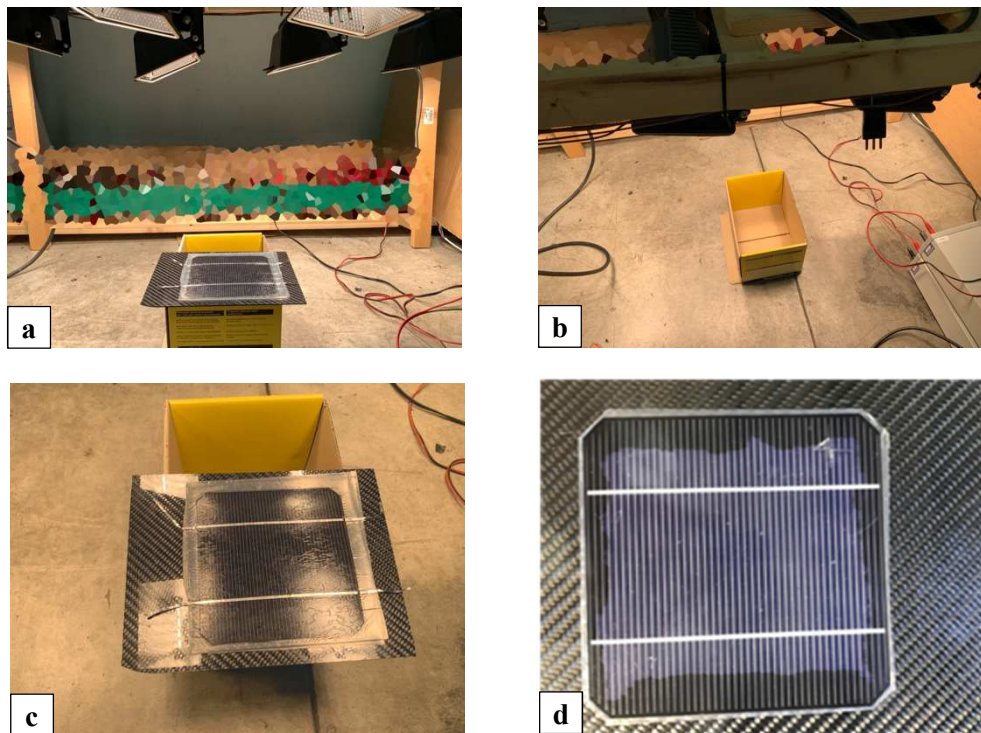


Fig. 3. Images from experiments: a) mock-up; b) details of the cardboard support; c) solar cell on supports and heated; d) detail of the solar cell on the CFRP panel.

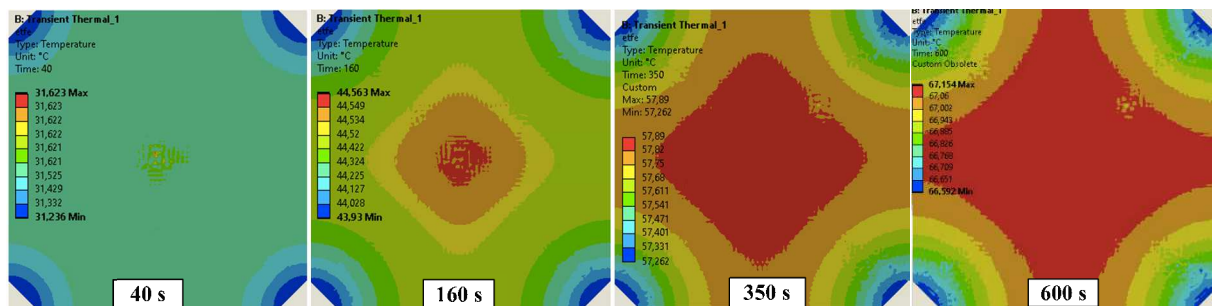


Fig. 4. Thermal evolution as simulated in the case of the 1st layout (i.e., reference layout) and the 3rd layer (i.e., silicon cell) for t = 40, 160, 350 and 600 seconds.

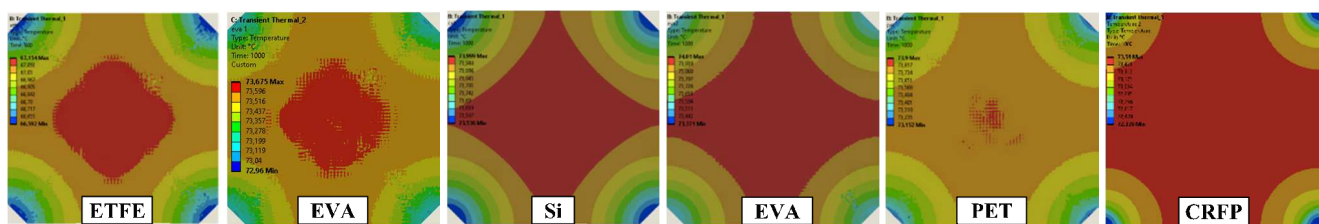


Fig. 5. Thermal differences through layer, in the case of the 1st layout at steady state (t > 1.000 sec).

4. Results and Discussion

4.1. Numerical results

Numerical simulations provided the evolution over the time of the expected thermal distribution. This information is available in each layer of each layout. For instance, fig. 4 shows the thermal evolution of a solar panel in four specific moments (t=40, 160, 350 and 600 sec.), as predicted in the case of the 3rd layer (i.e., silicon cell) of the 1st layout (i.e., reference layout). It is evident that the temperature quickly increases (31-> 44 -> 57 -> 67 °C) towards the equilibrium value (i.e., 73 °C for t > 1.000 sec). Moreover, in fig. 5 the thermal differences between the 7 layers are shown. The difficulty of a visual comparison is evident. This depends on the fact that the temperatures are well uniform on the surface and, consequently, the automatic color scales do not allow to obtain details. Therefore, comparison with respect to values (instead of color maps) was preferred.

Table 3 reports numerical results in terms of the maximum temperatures achieved in each layer per each different layout. These values represent the steady state and highlight a not-negligible variability.



Table 3. Simulation data: maximum layers' temperatures with respect to the different layouts.

Layer	Function	Material	Layout					$\Delta_{(max-min)}$
			1	2	3	4	5	
1 st	Frontsheet	ETFE	67.14	75.40	-	-	74.56	8.26
2 nd	Encapsulant	EVA	74.12	76.01	77.63	77.87	75.15	3.75
3 rd	Solar Cell	Silicon	73.99	77.26	77.80	77.96	75.15	3.97
4 th	Encapsulant	EVA	74.01	76.25	77.81	77.96	75.14	3.95
5 th	Backsheet	PET	73.90	-	77.70	77.96	-	4.06
6 th	Adhesive	Tape	73.59	76.08	77.40	77.74	75.15	4.15
7 th	Support	CFRP	73.59	76.07	77.40	77.73	75.14	4.14
$\Delta_{(max-min)}$			6.98	1.86	0.41	0.23	0.59	4.14
Density* (kg/m ³)			1.453	1.188	0.977	0.794	1.004	0.660

*Average Density Layers from 1st to 5th

According to the simulation, for instance, the maximum temperature:

- varies up to 4 °C between one layout and another for the silicon.
- varies quite little between layers (<1 °C), although there are interesting exceptions (≈2 and ≈7 °C)

Fig. 6 provides a direct comparison between (1st – 5th) layouts in terms of maximum layers' temperatures. It is evident, e.g., how halving EVA thickness (4th vs 3rd layouts) provides no thermal benefit but reductions in weight (-18.7%). Finally, backsheet removal can instead significantly reduce weight (40%), accepting a negligible temperature increase (+1 °C) of the panel (5th vs 1st layouts).

4.2. Experimental results

Experiments provided the thermography of samples over the time. For instance, in Fig. 7, the thermal evolutions in the case of the 1st layout (i.e., reference layout) as measured at t = 40, 160, 350 and 600 sec, are reported. A probe (i.e., the cross in the center) also provided the value of temperature in that spot. Because of the transparency of ETFE and EVA (respectively 1st and 2nd layer), it was assumed that the measured temperatures can be referred to the silicon cell (3rd layer). This assumption is also strengthened by the fact that, in agreement with the simulations, the differences between EVA and silicon (2nd and 3rd layers) are minimal.

From thermography several aspects can be noted:

- the heat flux is not completely homogeneous (as assumed in the simulation) with a slightly higher concentration on the left.
- even if this geometrical imbalance appears minimal (<25mm), the effect is evident, with the upper left quadrant heating up faster.
- linked to this non-uniform heating, the maximum temperature moves from the center to other areas of the panel.
- a difference emerges between the maximum temperature and the measured temperature at the center (≈ 5-6 °C).
- the local states along the boundary conditions on the border significantly affect the thermal distribution regularity.
- the cooling effect of the edge areas appears not uniform (as assumed in the simulation)

However, the effect of this non-uniformity is overcome measuring and confirming the irradiation value (1000 W/m²) at the center.

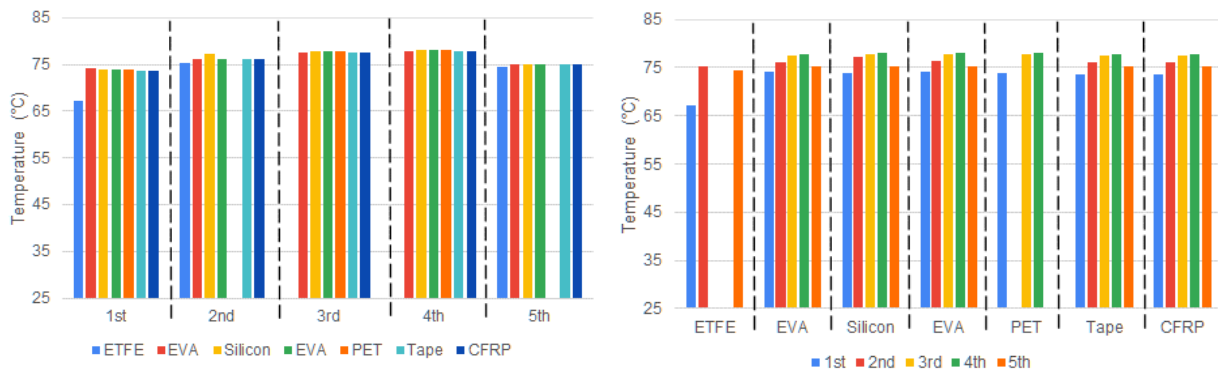


Fig. 6. Comparing maximum layers' temperatures in the different layouts.

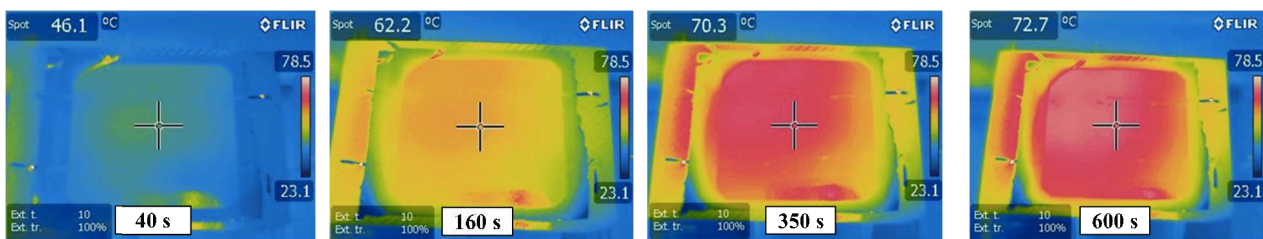


Fig. 7. Thermal evolution as measured in the case of the 1st layout (i.e., reference layout) and the 3rd layer (i.e., silicon cell) at t = 40, 160, 350 and 600 sec.



Table 4. Temperature of the solar cell at the midpoint: experiment vs simulation

Layout	1	2	3	4	5
Sample 1	67.6	75.1	76.2	78.7	81.2
Sample 2	72.7	74.7	77.0	80.3	81.4
Sample 3	73.4	76.1	78.3	80.6	81.7
Avg.	71.2	75.3	77.2	79.9	81.4
Dev.St.	±3.2	±0.7	±1.1	±1.0	±0.3
Simulation	73.2	75.4	77.8	78.0	75.5
Err%	2.8%	0.1%	0.8%	-2.3%	-7.3%

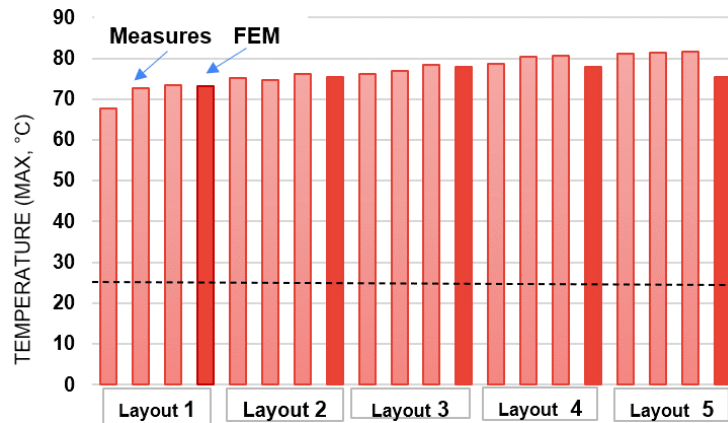


Fig. 8. Measured and predicted maximum temperatures on the silicon layer in each layout.

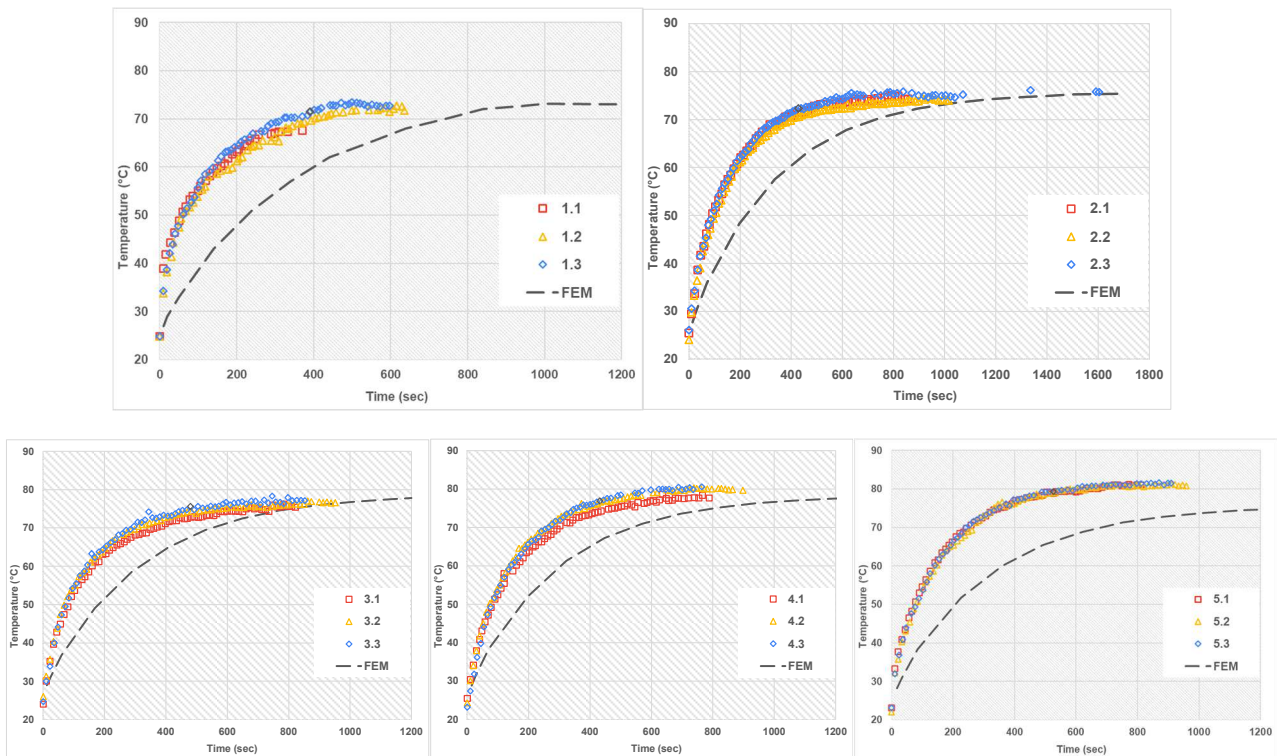


Fig. 9. Thermal transient analysis for each layout: measures vs simulation.

4.3. Steady state

Experimental measures and FEM predictions in the case of steady state conditions are shown in Fig. 8. They represent the three measured and one predicted values of temperature in the solar cell midpoint of the silicon layer (3rd layer) for the (five) stacking sequences under investigation. These values are also reported in Tab. 3, together with average, standard deviation, and percent error.

Regarding these values, between the most relevant aspects, it is possible to highlight:

- very low variability in measures, usually within a standard deviation of $\approx \pm 1^\circ\text{C}$ (equal to 1.5%), up to $\pm 3^\circ\text{C}$ (4%) in a single case.
- a range of 10 °C in the temperature on the silicon cell.
- numerical outputs accurately (err. <3%) predict the average temperatures in most cases (4 layouts out of 5).



4.4. Transition state

Experimental measures and numerical predictions in the case of transient conditions are shown in Fig. 9. Specifically, the graphs report the maximum temperature on the silicon layer (3rd layer) for the (five) layouts.

It is evident that, with respect to every layout, the three experimental curves (one per sample) overlap almost perfectly. The differences are limited to few degrees (°C), almost in line with the measured variations of the environmental temperature (T_{env}).

Regarding the simulations, even if the curves succeed in predicting the limit values (as mentioned regarding the steady-state), differences exist in the transient zone. Predictions seem to underestimate the ability of the system to rapidly accumulate heat, maybe related to the fact of not being able to correctly define the thermal insulation of the layers under the silicon.

5. Conclusion

The highest efficiency in solar energy conversion is a fundamental aspect wherever photovoltaic panels are present, but it is even more critical in the case of racing solar cars. Minimal losses in the conversion efficiency, which however remain present for the many hours of solar racing, can cause the solar car to lose several positions in the standings, especially influencing top vehicles.

The nominal power of photovoltaic panels usually refers to standard test conditions, with a solar radiation of 1,000 W/m², an air density of 1.5 kg/m³ and a temperature of the photovoltaic cells of 25 °C. In many cases, however, operational temperature conditions should be considered since the thermal coefficients of the panels can vary considerably. In the case of silicon panels, for instance, this change reaches the highest value between all different technologies, up to 0.5% /°C. It means that the efficiency of the panel can be reduced by 5% every 10 °C of temperature over the standard 25 °C. Therefore, in the presence of cell temperatures of 60°, the drop with respect to the nominal power values can reach up to 17-18%.

Here the goal was to improve performance by maximizing thermal dissipation thanks to proper design solutions, involving both the aspects of materials selection and layer thicknesses, for encapsulating monocrystalline silicon solar cells. In this numerical-experimental study, five functional stratifications of monocrystalline silicon cells were made and compared through a transient thermal analysis, validated thanks to experimental temperature measurements.

These results are very promising with a good prediction of temperatures in stationary conditions (less so in transient ones). In some cases, an extreme accuracy was obtained with errors of the order of 0.1-0.8%. Even when lower (7%), the accuracy is enough for an appropriate model utilization.

This kind of information allows finding the right compromise in the cell layout design between the lowest temperature on the cells able to guarantee the highest conversion efficiency and the structural lightness, which cannot be reduced at will, given the functional purposes of each material layers. For instance, it was possible to conclude that a remarkable design option consists in the removal of the last layer (i.e., PET backsheet) to significantly lighten (-40%) the solar panel. This is possible only if the panel is properly inserted in the vehicle design [34, 35] considering a convenient support and protective structure.

The aim of the work, however, was not so much to choose the best one among the specific construction hypotheses of the photovoltaic modules investigated here, but above all to set up an efficient numerical model for solar cell design. Thanks to this new validated model, in fact, it is now possible to easily investigate the behavior of the alternative solar panels in conditions closer to the ones expected from reality. In this sense, different and more complex boundary conditions are awaited [36] in the case of the solar vehicle such as: the true three-dimensional geometry of the roof, the angle of incidence of the sun in its different positions, the presence of EV modules side by side, air speeds while the vehicle is moving [37]. Moreover, in terms of vehicle design optimization, the new numerical model allows to verify the effect of aspects such as the use of different geometries and materials in the solar panel housing structure, as well as the actual usefulness of different passive and active cooling hypotheses proposed by the designers.

Author Contributions

C. Fragassa planned the research scheme and resources, suggested the experiments and simulations, supervised the project; A. Pavlovic initiated the activity and, together with C. Fragassa defined methods and materials; M. Bertoldi, supported by V. Mikhnych, designed, conducted the experiments, and analyzed the empirical results; A. Pavlovic developed the numerical modeling, performed the simulations, examined the validation. The manuscript was written by C. Fragassa in its draft version, then helped by the other authors for its finalization. All authors discussed the results, reviewed, and approved the final version of the manuscript.

Acknowledgments

Special thanks to Prof. Bryce Richards (Karlsruhe Institute of Technology) and Prof. Frank Wagner (Aix-Marseille University) for supporting the initiative.

Conflict of Interest

The authors declared no potential conflicts of interest with respect to the research, authorship, and publication of this article.

Funding

This research was carried out within the international collaboration project 'Two Seats for a Solar Car', an intervention funded by the Italian Ministry of Foreign Affairs and International Cooperation (MAECI) with the scope to convert a racing solar car into a solar road vehicle. Methodological and technological results are exploited inside the Central European Initiative framework (as part of the 'Composite for All' and 'ATC.EVO' transfer of technology actions).


References


- [1] Kumar, R. R., Alok, K., Adoption of electric vehicle: A literature review and prospects for sustainability, *Journal of Cleaner Production*, 253, 2020, 119911.
- [2] Rapa, M., Gobbi, L., Ruggieri, R., Environmental and Economic Sustainability of Electric Vehicles: Life Cycle Assessment and Life Cycle Costing Evaluation of Electricity Sources, *Energies*, 13, 2020, 6292.
- [3] Rizzo, G., Arsie, I., Sorrentino, M., *Hybrid solar vehicles*. INTECH Open Access Publisher, 2010.
- [4] Araki, K., Ji, L., Kelly, G., Yamaguchi, M., To do list for research and development and international standardization to achieve the goal of running a majority of electric vehicles on solar energy, *Coatings*, 8(7), 2018, 251.
- [5] Ross, V., Solar-powered vehicles: Race to the bottom, *Ecogeneration*, 103, 2017, 42-43.





- [6] Betancur, E., Osorio-Gómez, G., Rivera, J. C., Heuristic optimization for the energy management and race strategy of a solar car, *Sustainability*, 9(10), 2017, 1576.
- [7] Minak, G., Fragassa, C., de Camargo, V.F., A Brief Review on Determinant Aspects in Energy Efficient Solar Car Design and Manufacturing, *Smart Innovation, Systems and Technologies*, 68(14.6), 2017, 847-856.
- [8] Geisz, J. F., France, R. M., et al., Six-junction III-V solar cells with 47.1% conversion efficiency under 143 Suns concentration, *Nature Energy*, 5(4), 2020, 326-335.
- [9] Yamaguchi, M., Masuda, T., et al., Role of PV-powered vehicles in low-carbon society and some approaches of high-efficiency solar cell modules for cars, *Energy and Power Engineering*, 12(06), 2020, 375.
- [10] Koyuncu T., Practical Efficiency of Photovoltaic Panel Used for Solar Vehicles, *IOP Conf. Ser.: Earth Environ. Sci.*, 83, 2017, 012001.
- [11] Skoplaki, E., Palyvos, J., On the Temperature Dependence of Photovoltaic Module Electrical Performance: A Review of Efficiency/ Power Correlations, *Solar Energy*, 83, 2009, 614-624.
- [12] Evans, D. L., Simplified method for predicting photovoltaic array output, *Solar Energy*, 27(6), 1981, 555-560.
- [13] Green, M. A., *Solar cells: Operating principles, technology, and system applications*, Englewood Cliffs, 1982.
- [14] Incropera P.F., De Witt P.D., *Fundamentals of heat and mass transfer (5th edition)*, John Wiley and Sons, 2002, ISBN 0-471-38650-2.
- [15] Park, Y., Jung, T., Go, S., Ju, Y., Kim, J., Kang, G., Prediction of temperature distribution in PV module using finite element method, *Materials Science*, 2016, 113438890.
- [16] Mavromatakis, F., Kavoussanaki, E., Vignola, F., Franghiadakis, Y., Measuring and estimating the temperature of photovoltaic modules, *Solar Energy*, 110, 2014, 656-666.
- [17] Korkut, T. B., Goren, A., Ezan, M. A., A CFD study on photovoltaic performance investigation of a solar racing car. In *Environmentally-Benign Energy Solutions*, 2020, 509-529.
- [18] Sánchez Barroso, J. C., Barth, N., Correia, J. P. M., Ahzi, S., Khaleel, M. A., A computational analysis of coupled thermal and electrical behavior of PV panels, *Solar Energy Material and Solar Cells*, 148, 2016, 73-86.
- [19] Zhou, J., Yi, Q., Wang, Y., Ye, Z., Temperature distribution of photovoltaic module based on finite element simulation, *Solar Energy*, 111, 2015, 97-103.
- [20] Chou, T.-L., Shih, Z.-H., Hong, H.-F., Han, C.-N., Chiang, K.-N., Investigation of the thermal performance of high-concentration photovoltaic solar cell package, in *2007 International Conference on Electronic Materials and Packaging*, Nov. 2007, DOI: 10.1109/EMAP.2007.4510295.
- [21] Chen, W.-H., Cheng, H.-C., Shen, H.-A., An effective methodology for thermal characterization of electronic packaging, *IEEE Transactions on Components, Packaging and Manufacturing Technology*, 26(1), 2013, 222-232.
- [22] Minak, G., Brugo, T., Fragassa, C., Pavlovic, A., Zavatta, N., De Camargo, V.F. Structural Design and Manufacturing of a Cruiser Class Solar Vehicle, *Journal of Visualized Experiments*, 143, 2019, 58525.
- [23] Pavlovic, A., Sintoni, D., Fragassa, C., Minak, G., Multi-Objective Design Optimization of the Reinforced Composite Roof in a Solar Vehicle, *Applied Sciences*, 10, 2020 2665.
- [24] Pavlovic, A., Sintoni, D., Minak, G., Fragassa, C., On the Modal Behaviour of Ultralight Composite Sandwich Automotive Panels, *Composite Structures*, 248, 2020, 112523.
- [25] Ethylene Tetrafluoroethylene (ETFE): MakeItFrom.com. <https://www.makeitfrom.com/material-properties/Ethylene-Tetrafluoroethylene-ETFE>. (Accessed Apr. 28, 2021).
- [26] Ethylene Vinyl Acetate (EVA): MakeItFrom.com. <https://www.makeitfrom.com/material-properties/Ethylene-Vinyl-Acetate-EVA> (Accessed Apr. 28, 2021).
- [27] Lee, B., Liu, J. Z., Sun, B., Shen, C. Y., Dai, G.C. Thermally conductive and electrically insulating EVA composite encapsulant for solar photovoltaic (PV) cell, *Express Polymer Letters*, 2(5), 2008, 357-363.
- [28] France-Lanord, A., Merabia, S., Albaret, T., Lacroix, D., Termentzidis, K., Thermal properties of amorphous/crystalline silicon superlattices, *Journal of Physics: Condensed Matter*, 26(35), 2014, d355801.
- [29] Abe, H., Kato, H., Baba, T., Specific Heat Capacity Measurement of Single-Crystalline Silicon as New Reference Material, *Japanese Journal Applied Physics*, 50(11), 2011, 11RG01.
- [30] Polyethylene terephthalate - online catalogue source - supplier of research materials in small quantities - Goodfellow. <http://www.goodfellow.com/E/Polyethylene-terephthalate.html> (accessed Apr. 29, 2021).
- [31] Overview of materials for Polyethylene Terephthalate (PET), Unreinforced. <http://www.matweb.com/search/DataSheet.aspx?MatGUID=a696bdcdff6f41dd98f8e3599eaa20ckck=1> (accessed Apr. 29, 2021).
- [32] Zheng, X., Kim, S., Park, C. W., Enhancement of thermal conductivity of carbon fiber-reinforced polymer composite with copper and boron nitride particles, *Composites Part A: Applied Science and Manufacturing*, 121, 2019, 449-456.
- [33] 3M Industrial Adhesives and Tape. Solutions for your assembly challenges, 2019, <https://multimedia.3m.com/mws/media/10159040/3m-industrial-adhesives-and-tapes.pdf>.
- [34] Ali, H. T., Akrami, R., Fotouhi, S., Pashmforoush, F., Fragassa, C., Fotouhi, M., Effect of the stacking sequence on the impact response of carbon-glass/epoxy hybrid composites, *Facta Universitatis, Series: Mechanical Engineering*, 18(1), 2020, 69-77.
- [35] Fragassa, C., Pavlovic, A., Minak, G., On the structural behaviour of a CFRP safety cage in a solar powered electric vehicle, *Composite Structures*, 252(15), 2020, 112698.
- [36] Sobamowo, G., Finite element thermal analysis of a moving porous fin with temperature-variant thermal conductivity and internal heat generation, *Reports in Mechanical Engineering*, 1(1), 2020, 110-127.
- [37] Mohamad, B., Karoly, J., Zelentsov, A., CFD Modelling of Formula Student Car Intake System, *Facta Universitatis, Series: Mechanical Engineering*, 18(1), 2020, 153-163.

ORCID iD

Ana Pavlovic  <https://orcid.org/0000-0003-2158-1820>

Cristiano Fragassa  <https://orcid.org/0000-0003-0046-8810>

Marco Bertoldi  <https://orcid.org/0000-0002-6188-2751>

Vladyslav Mikhnych  <https://orcid.org/0000-0003-4930-848X>



© 2021 Shahid Chamran University of Ahvaz, Ahvaz, Iran. This article is an open access article distributed under the terms and conditions of the Creative Commons Attribution-NonCommercial 4.0 International (CC BY-NC 4.0 license) (<http://creativecommons.org/licenses/by-nc/4.0/>).

How to cite this article: Pavlovic, A., Fragassa, C., Mikhnych, V., Bertoldi, M. Thermal Behavior of Solar Cell Encapsulation Materials: A Numerical and Experimental Investigation, *J. Appl. Comput. Mech.*, 7(3), 2021, 1847-1855. <https://doi.org/10.22055/JACM.2021.37852.3101>

Publisher's Note Shahid Chamran University of Ahvaz remains neutral with regard to jurisdictional claims in published maps and institutional affiliations.

